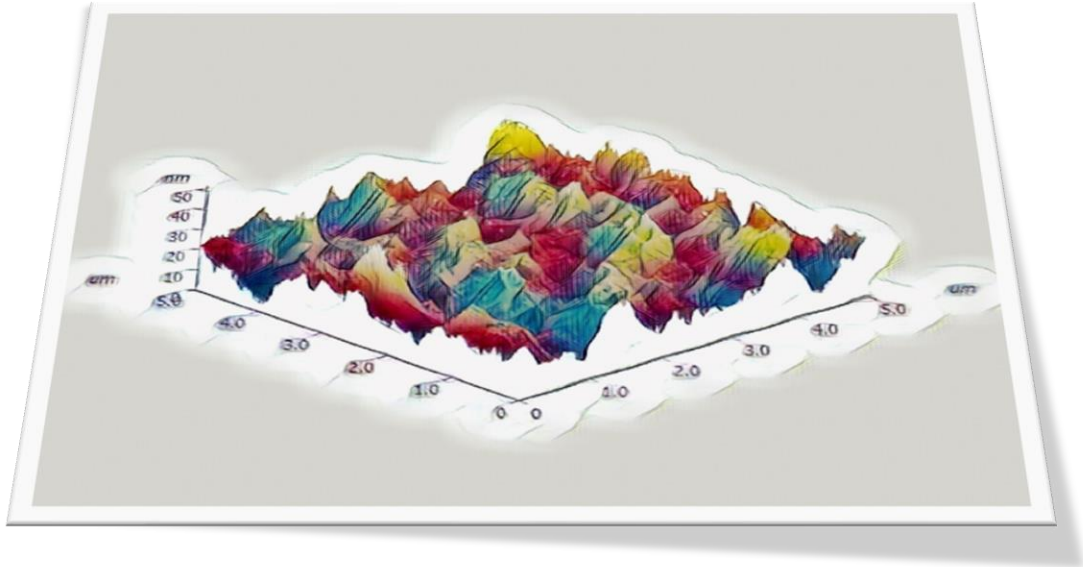# Chapter 2

Experimental (material and methods) and Characterization Techniques

Chapter 2: Experimental (material and methods) and Characterization Techniques

2.1 Introduction

This chapter is dedicated to the synthesis process techniques and material characterization techniques used in this work. The synthesis of the polymer nanocomposite is discussed in detail. Preparation of the filler to reinforce in the polymer matrix is done with solvothermal process and mechanochemical synthesis process. We have synthesized the five types of the filler as Nitrogen doped carbon dots (N-CDs), V_2O_5, Hydrated antimony pentoxide (HAP), $LaFeO_3$ and $GdFeO_3$. The synthesis of the N-CDs has been done with the help of the solvothermal process. The nano powder of the V_2O_5, Sb_2O_3, $LaTiO_3$ and $GdFeO_3$ was done with the help of the mechanochemical process. Further, the hydroxylation of the all filler excluding the N-CDs was done to make better nanocomposite. Hydroxylation gave us the final nanofillers Hydroxylated V_2O_5 (Hy- V_2O_5), HAP, Hy-$LaTiO_3$, Hy-$GdTiO_3$ ready to reinforcement. The synthesis of the polymer nanocomposite film was done with the help of the solution cast process. We have synthesized pure PVDF and PVDF based nanocomposite films with the varying concentration in matrix of the nanofillers.

The X-Ray diffraction pattern of samples was recorded using the Rigaku Miniflex X-Ray Diffractometer. FTIR was done with the help of Alpha Bruker Eco-ATR in the spectral range of 400 to 1400cm^{-1}. A JASCO V-650 UV-visible spectrophotometer was used to measure the absorption spectra and determination of band gap of the filler. Thermal degradation analysis of composite films was done by TGA and DSC measurements using DSC-60 Plus, M/s Shimadzu (Asia Pacific) Pte Ltd under the nitrogen atmosphere. Microstructural and morphological investigations of the surface of all composite films were done using a high-resolution Scanning Electron Microscope (HR-SEM, FEI, NOVA NANOSEM 450). Scanning Probe Microscopy

(SPM) was done by NTEGRA Prima, NT-MDT. Elemental analysis was done with the help of X-ray photoelectron spectroscopy (XPS) (K-Alpha, Thermo Fisher Scientific). The dielectric constant was measured on fast-drying (room temperature) silver paint electroded nanocomposite films with the help of the Novocontrol Alpha-A high performance frequency analyzer in the range of 30°C to 120°C temperature at the frequency range of 1MHz to 1kHz. The data was collected with the help of Win-data software. The dielectric measurement was also done with the help of the Keysight B2912A Precision Source / Measure Unit (SMU). The electroded composite films were further characterized for Polarization vs electric field hysteresis loop with the help of Radiant technology precision premier-II materials using the bipolar sine wave of frequency (10Hz). For the electrical breakdown strength measurement for Weibull analysis, we used an AC dielectric strength breakdown test set-up.

2.2 Materials and Methods

2.2.1 Precursor

Poly (vinylidene fluoride) PVDF (Alfa Aesar, 99.9%), N, N- Dimethylformamide (DMF) purchased from Merck chemicals, Citric acid (Alfa Aesar, 99.9%), Urea (Alfa Aesar, 99.9%), H_2O_2 (50%) Merck Millipore, Deionized Water, High purity V_2O_5 (99.9%) powder was purchased from sigma Aldrich with ~45 μm, Sb_2O_3 (99.9%, Sigma Aldrich), La_2O_3 (Sigma-Aldrich, 99.9%), Gd_2O_3 (Sigma-Aldrich, 99.9%), Fe_2O_3 (Sigma-Aldrich, 99.9%).

Table 2.1 The properties of the PVDF matrix and the fillers to be used.

Matrix	Melting point (°C)	Dielectric constant (1kHz)	Density (g/cm^3)
PVDF	140-160	7-9	1.78
Nanofiller	Optical band gap (eV)	Dielectric constant (1kHz)	Density (g/cm^3)

V_2O_5	2.3	4.6	3.36
Sb_2O_3	3.2-3.7	-	5.2
$LaFeO_3$	2.31-2.46	~270	6.4
$GdFeO_3$	0.32	~590	7.3
N-CDs	3.0	~3 (N-GQDs)	-

2.2.2 Synthesis of nanofiller

Synthesis of the nanofiller is done with the solvothermal process and mechanochemical process.

2.2.2.1 Solvothermal process to synthesis the nanomaterials

Solvothermal synthesis is a chemical process that takes place in a solvent other than water at a temperature above the boiling point of the solvent in a closed container[78]. The vessel or container is made up of Teflon coated and put under the steel container. Precise control of the parameters of the reaction inside the vessel helps in getting desired particle size and shape distribution. We have used the DMF as the solvent in this process. The container is of the 100ml with operating temperature range up to 250°C. The autoclave is put in furnace or oven for the required period of time with appropriate precursors. The dark product is centrifuged until the bigger particles are settle on the bottom and light transparent product is final nanoparticles. The Figure 2.1 shows the schematic diagram of the solvothermal process.
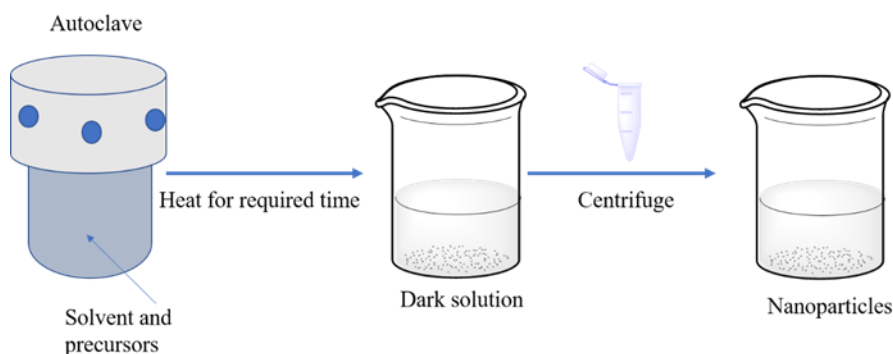
Figure 2.1 Schematic of the solvothermal process

2.2.2.2 Mechanochemical process (High energy ball milling).

High-energy ball milling is a mechanical deformation process that is frequently used for producing nanocrystalline powder of oxides[79]. In the mechanochemical milling process, granular structures undergo segregation as the result of severe cyclic deformation induced by milling with hard balls in a high-energy ball mill. This process has been successfully used to produce oxide nanocrystalline powder with minimum particle sizes from 10 to 50 nm. The high-energy ball milling technique is straightforward and has high capability to synthesize at large scale. The bulk oxide powders are put in the jars of the ball milling machine with the 3mm ball in the weight ratio of 3:1 in ethanol solvent. The time of ball milling is done as according to the required size of the particles. The mixture is further dried until the ethanol vaporized. The Figure 2.2 shows the schematic diagram of the mechanism happening inside the ball milling containers
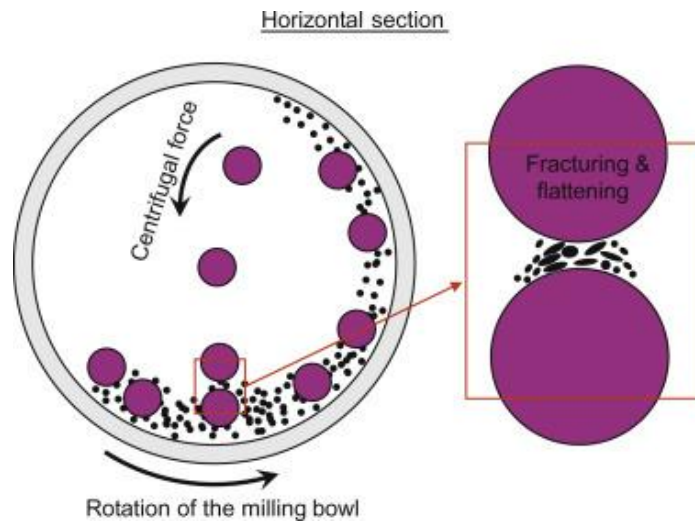
Figure 2.2 Schematic diagram of the mechanism inside the high energy ball mill [79].

2.2.2.3 Hydroxylation process of the nanoparticles

The hydroxylation is the process by which, -OH is added to the nanoparticles to make better polymer nanocomposite by improving dispersion of the surface modified nanoparticles in the polymer matrix [69]. In this process, to hydroxylate the nano powder, the H_2O_2 is taken as 30% of the water and particular weight percentage ratio of the nano powder is taken and further, the process is completed as shown in the Figure 2.3.
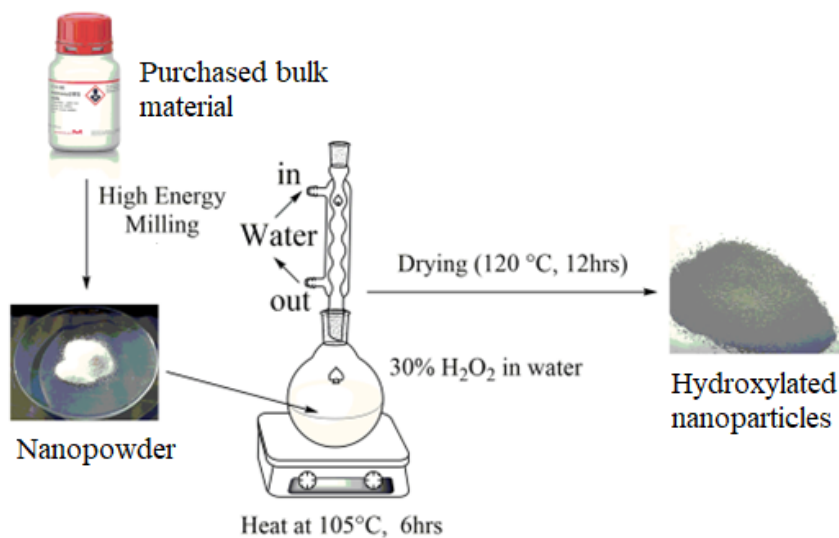

Figure 2.3 Schematic diagram of the hydroxylation of nanoparticles

2.2.3   Synthesis of Polymer nanocomposite via solution cast method

In this method, polymer is poured in a solvent that can make solution with. The polymer is acts as matrix that is partially or fully soluble, whereas the nanoparticles are dispersed in same solvent or different solvent to make a mixture or suspension [80]. The dispersed nanoparticles are mixed in the solution of the polymer for the required time and then solution is casted and dried. We have used the DMF as the common solvent in the synthesis process of the film. Nanoparticles are primarily probe sonicated to avoid aggregation inside the polymer matrix and then stirred as shown in the Figure 2.4 which shows the whole process.

Advantages of Solution Cast Method

- Facile, cost effective and suitable for large scale production.

- Better uniformity of thickness and better clarity than extrusion.

- Synthesis at low temperatures that is valuable for thermally activated films or applications incorporating temperature-sensitive active ingredients.

- Additives and fillers may be incorporated more easily.

- Significant diversity in film thickness, now spanning from over 150 microns to under 20 microns.
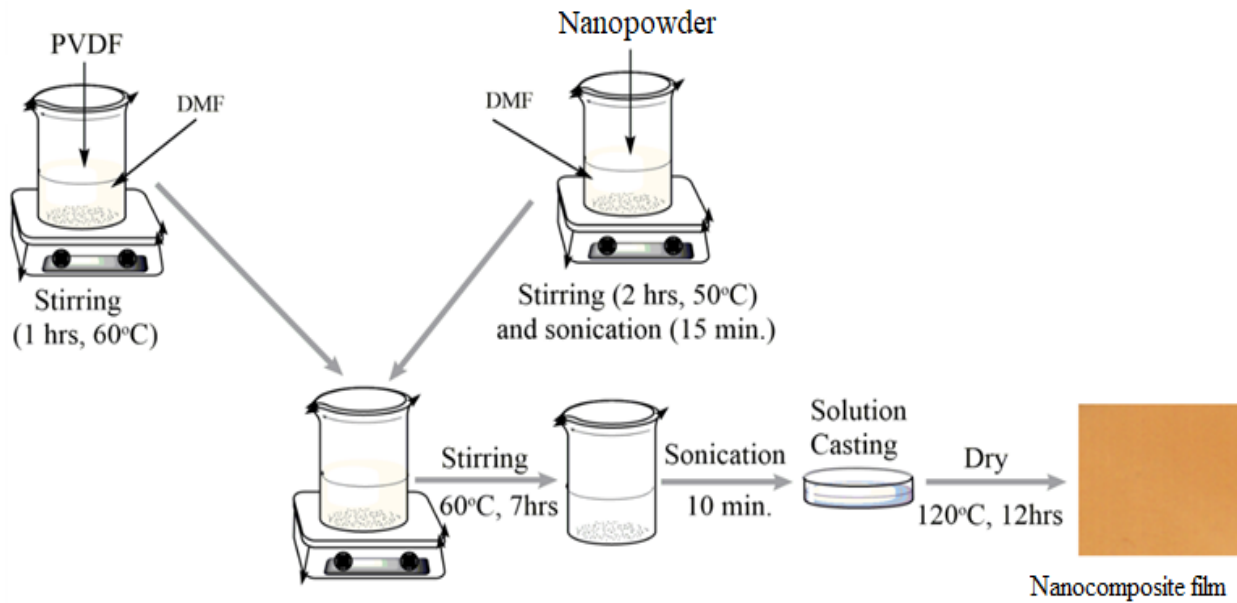
Figure 2.4 Solution cast method of the nanocomposite film

2.3   Characterization techniques

2.3.1   Powder X-ray diffraction (XRD)

Powder X-ray diffraction (XRD) analyzes the crystallographic phase and structural features of materials. Non-invasive approach for studying crystalline materials' structures, XRD identifies phases in unknown materials and structural and phase purities in novel materials. Incoming X-rays are deflected by parallel planes of atoms in a crystal. Crystals have angstrom-order atomic spacing, so X-rays are employed to examine the crystalline structure. Coherent X-ray scattering occurs when X-rays hit a specimen. The specimen's 'fingerprint' is the intensity and spatial distribution of dispersed X-rays. Bragg's law relates diffraction to material structure. Mathematically, Bragg's law is $2d_{hkl} \sin\theta = n$, where d_{hkl} is the interplanar lattice spacing, θ is the diffraction angle, is the X-ray wavelength, and n is the order of diffraction. Different peaks in the x-ray diffraction pattern are compared with a standard pattern (JCPDS/ICDD file) to determine the material's phase and crystal structure [81]. For unknown materials, diffraction patterns index crystal systems and lattice properties. XRD is used to characterize as-prepared

perovskite solid solutions. Powder XRD measurements were performed at room temperature from 10⁰ to 80⁰ using Cu-K-radiation (RIGAKU Smart Lab and MINIFLEX 600). J.R. Carvajal (1993) used Rietveld refinement to analyze the crystal structure. GIXRD is used for thin films. Grazing incidence is a sort of diffraction geometry in which incident rays are diffracted almost in the film's plane. Figure 2.5 shows the Bragg's law for X-Ray diffraction schematic diagram, image of the instrument and X-Ray diffraction of the PVDF and its nanocomposite.
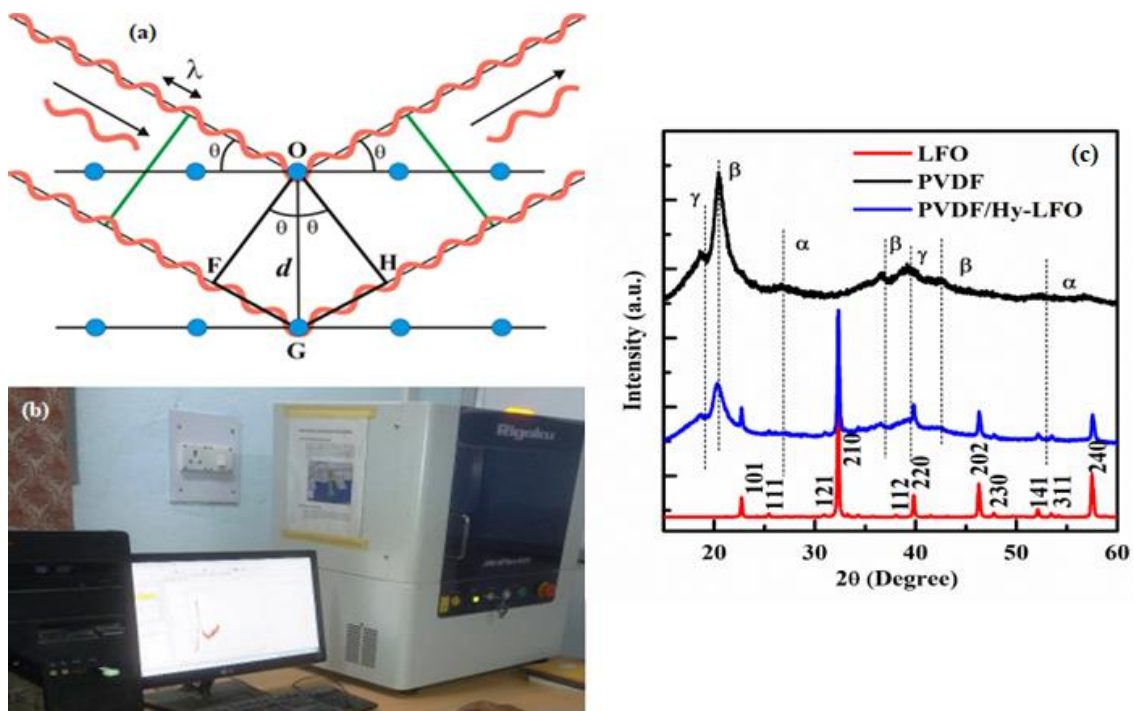

Figure 2.5 (a) Bragg's law for X-Ray diffraction schematic diagram, (b) Image of the instrument and X-Ray diffraction of the PVDF and it's nanocomposite.

2.3.2 Differential Scanning Calorimetry (DSC)

The Differential Scanning Calorimeter (DSC) is a powerful and adaptable tool that can test the thermal properties of a wide variety of materials at various temperatures. The Figure 2.6 shows the plot of the data showing the interpretation and instrument image. It monitors the heat flow and temperature as a function of time and temperature as a material change from one phase to another [82]. It determines the phases-changing processes of the materials and offers quantitative and qualitative data on endothermic (heat absorption) and exothermic (heat evolution)

processes. Additionally, it provides details on melting, glass transitions, crystallization, and oxidation, which are used to assess processing needs and performance for final applications.
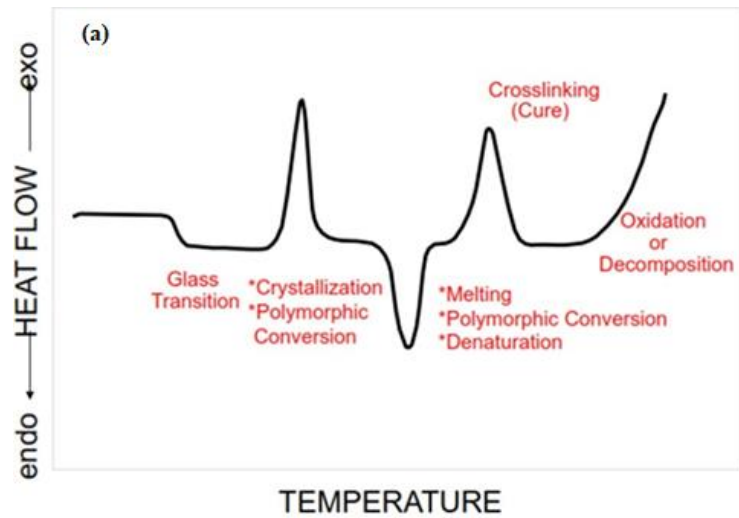

Figure 2.6 (a) DSC Graph and (a)Instrument.

2.3.3 X-ray photoelectron spectroscopy (XPS)

X-ray photoelectron spectroscopy (XPS) is a useful instrument for studying surface chemistry and bonding or identifying dopants in carbon nanomaterials. Photoelectric effect is XPS's foundation. First, an x-ray photon absorbs energy from core electron with lower energy. The excited target atom emits a photoelectron, forming a core hole [83]. The photoelectrons then hit

the to surface of the materials and escapes into the vacuum, where electrons kinetic energy is measured. Since carbon core electrons are not participate in the chemical reaction, core level signals should have small line-widths. Several factors cause signal broadening and shape changes. In any XPS measurement configuration, there is an inherent energy spread of the X-ray source, as well as a limited energy resolution of the analyzer. This combination of factors results in instrumental broadening. Non-monochromatic x-ray sources make it harder to create appropriate references. Finite sample temperature produces thermal broadening due to phonon vibrations, but this is generally minimal (since the thermal energy is only 25 meV at 300 K). Each peak has a natural line-width related to excited state lifespan, defined by a Lorentzian profile. Thus, a convolution of Gaussian (G) and Lorentzian (L) profiles, called Voigtian (V), best describes the characteristic forms, IV(E), of photoemission responses, where G(E) and L(E) are the Gaussian and Lorentzian contributions, is the instrumental widening, and is the intrinsic lifetime broadening. In graphite, graphene, or metallic carbon nanotubes, the carbon 1s line exhibits strong asymmetry towards higher binding energies. Many low-energy electron–hole couples screen the core hole, resulting in greater binding energy events. First, focus on the carbon 1s response to analyze contributions to the spectrum from synthesis by-products or carbonaceous pollutants. This is needed to assess dopant core states, 1s for nitrogen or 1s for oxygen. The Figure 2.7 shows the instrument image with schematic diagram and output data plot survey of the particular sample.
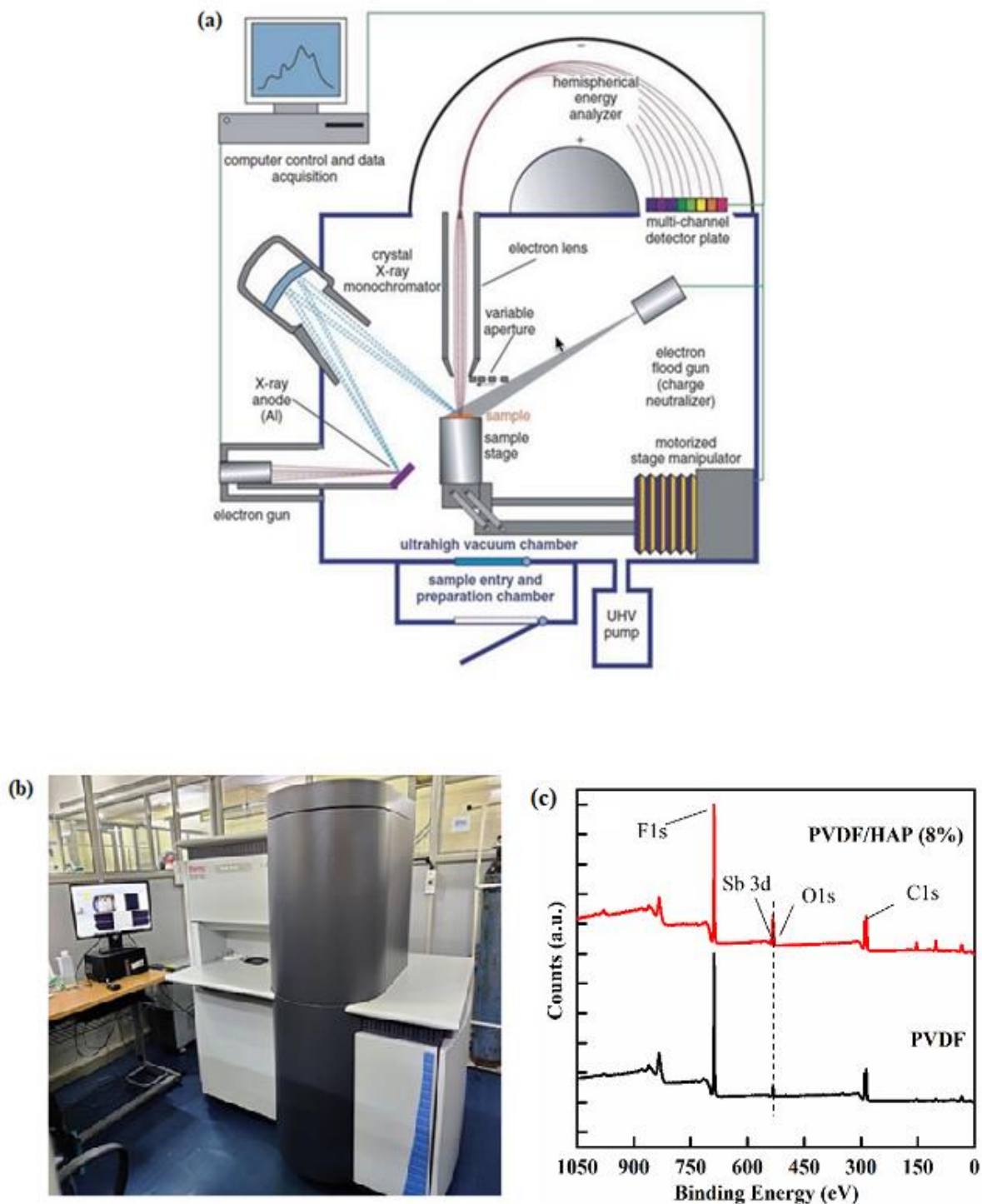
Figure 2.7 (a) Schematic diagram of mechanism of XPS, (b) XPS Instrument, (c) XPS Survey of PVDF/HAP.

2.3.4 Photoluminescence spectroscopy

Light spectroscopy, also known as PL spectroscopy, is performed when a substance emits light after being excited by a source of light energy (a photon). To put it simply, it is a method of

material testing that does not involve touching or otherwise damaging the sample being tested. The basic idea is to shine a beam of light over a sample such that it can absorb the light and undergo photo-excitation. Photo-excitation induces an instantaneous transition to a higher electronic state, followed by the emission of energy (photons) as the material returns to its original, lower energy state upon relaxation. Photoluminescence (PL) refers to the light or luminescence emitted by such a process [84]. The Figure 2.8 shows the schematic diagram of the instrument diagram, image of the photoluminescence spectroscopy and output data plot.
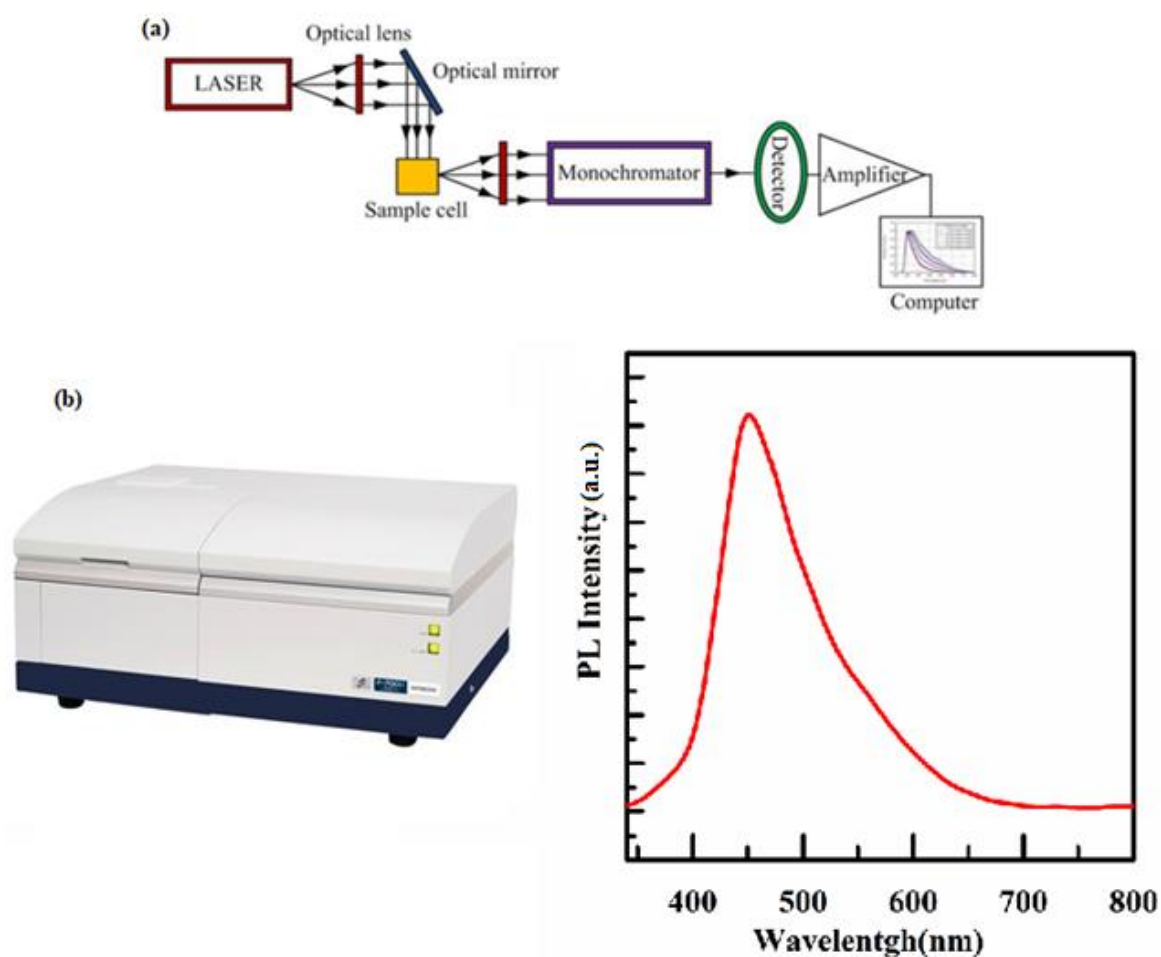
Figure 2.8 (a) Schematic of photoluminescence spectroscopy, (b) instrument diagram and (c) output data UV-Vis of N-CDs.

2.3.5   Scanning Electron Microscopy

SEM images of a synthesized materials were taken (ZEISS, Evo 18 Research). SEM scan surfaces of sample with a concentrated stream of electrons. Electrons hitting a sample's surface interact with atoms. Secondary electrons, backscattered electrons, and other signals are gathered, amplified, and detected by a scintillator-photomultiplier detector. The gathered data are translated into electrical signals and the scan is utilized to produce a picture of the material's surface. EDS-SEM offers to analyze the material's chemical composition, element presence, and concentration. EDS analyses X-rays from many elements simultaneously for reliable compositional analysis. An EDS X-ray spectrum allows us to quantify the elements in the electron-beam-irradiated object[85]. An electron beam stimulates materials in an EDS spectroscopy. Each element in the examined material creates particular X-ray energies based on inner orbital energy differences, which helps identify the components. High-resolution SEM images thin film cross-sections. Nova Nano SEM 450, FEI Company of USA (S.E.A.). The Figure 2.9 shows the schematic ray diagram of the FESEM, image of the FESEM instrument and FESEM image of the Sb_2O_3.
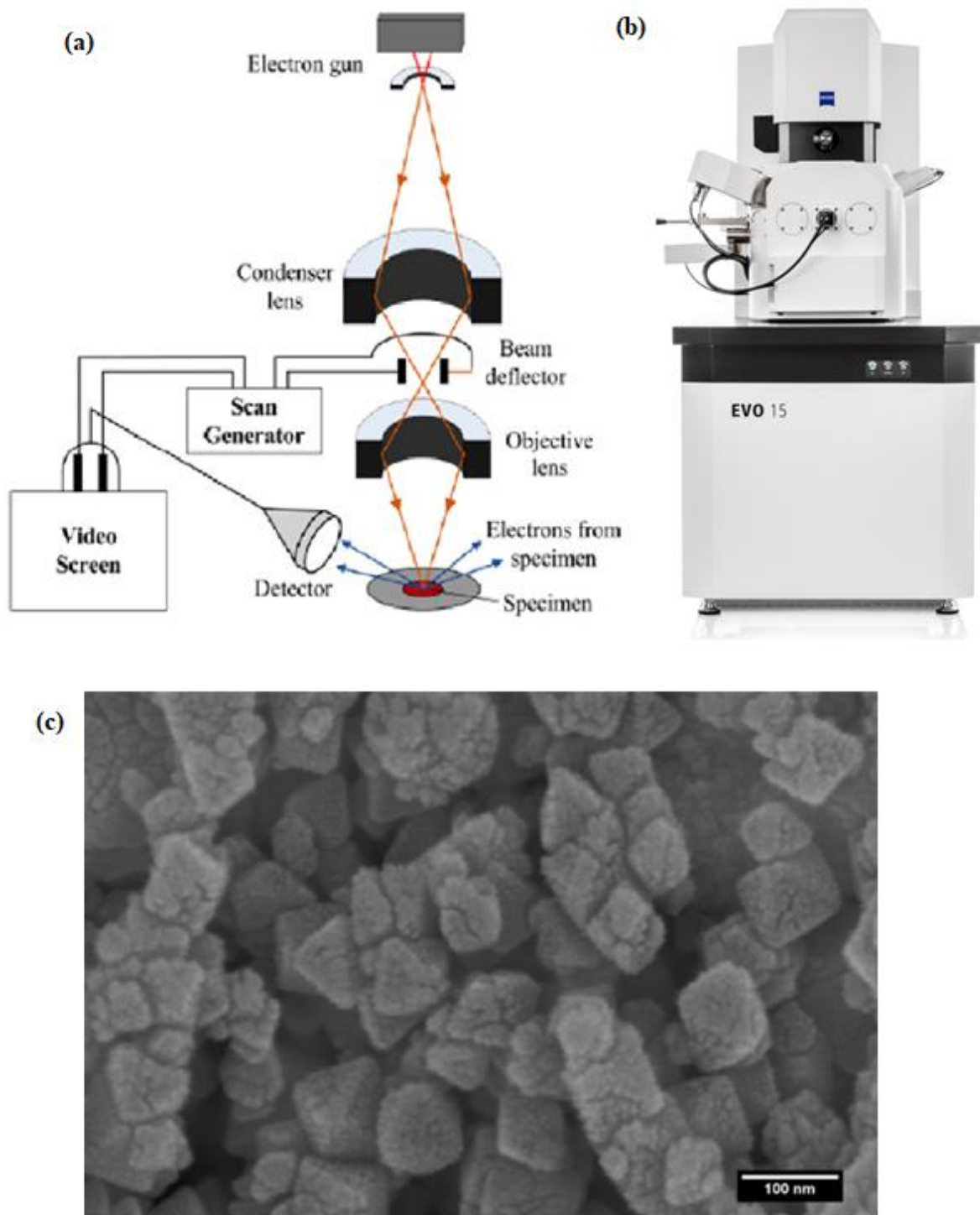
Figure 2.9 (a) Ray diagram for SEM with (b) image of the EVO - Scanning Electron Microscope MA15 / 18 CARL ZEISS MICROSCOPY LTD and (c) The FESEM image of the Sb_2O_3 nanoparticles.

2.3.6   **Transmission Electron Microscopy**

Transmission electron microscopy (TEM) is another significant characterization method. Signals are formed when a focused electron beam passes through a narrow piece of material. Magnetic lenses regulate and concentrate the electron beam from a tungsten filament or LaB6-based electron cannon. The whole microscope column and sample chamber operate under high vacuum to prevent electron scattering or discharge. TEM features imaging and diffraction modes. In imaging mode, a succession of projector lenses magnifies the sample picture in the objective's image plane. In diffraction mode, the diffracted beam generates the diffraction pattern in the rear focal plane of the objective lens, which is then multiplied by projector lenses to form the final diffraction pattern on the screen. SAED measures lattice constants, orientation, and other crystallographic data. TEM-FEI " Technai 20U Twin with EDX and Technai 20G2 at 200KeV" was utilized [86]. The ray diagram of the HRTEM is shown in the Figure 2.10. The Figure 2.11 shows the image of the HRTEM and TEM micrograph of the N-CDs.
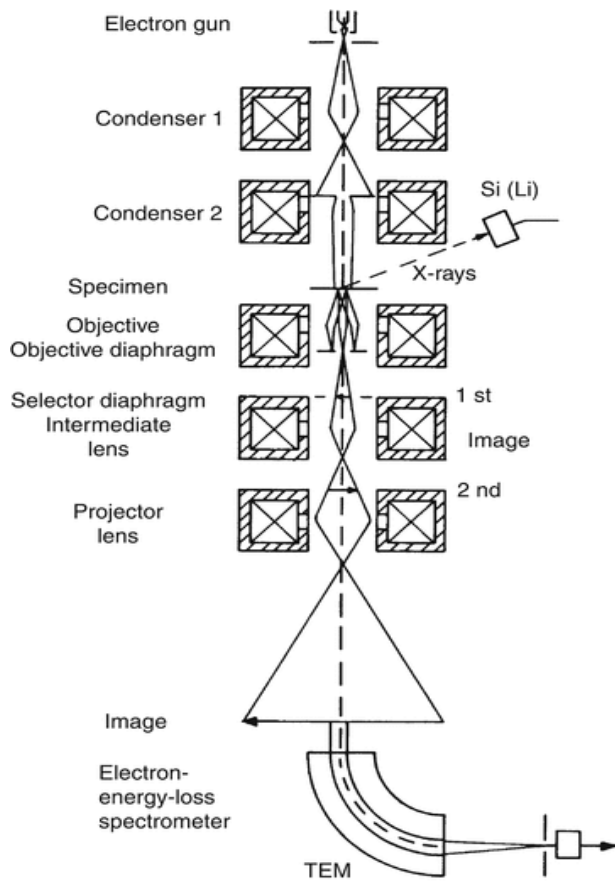
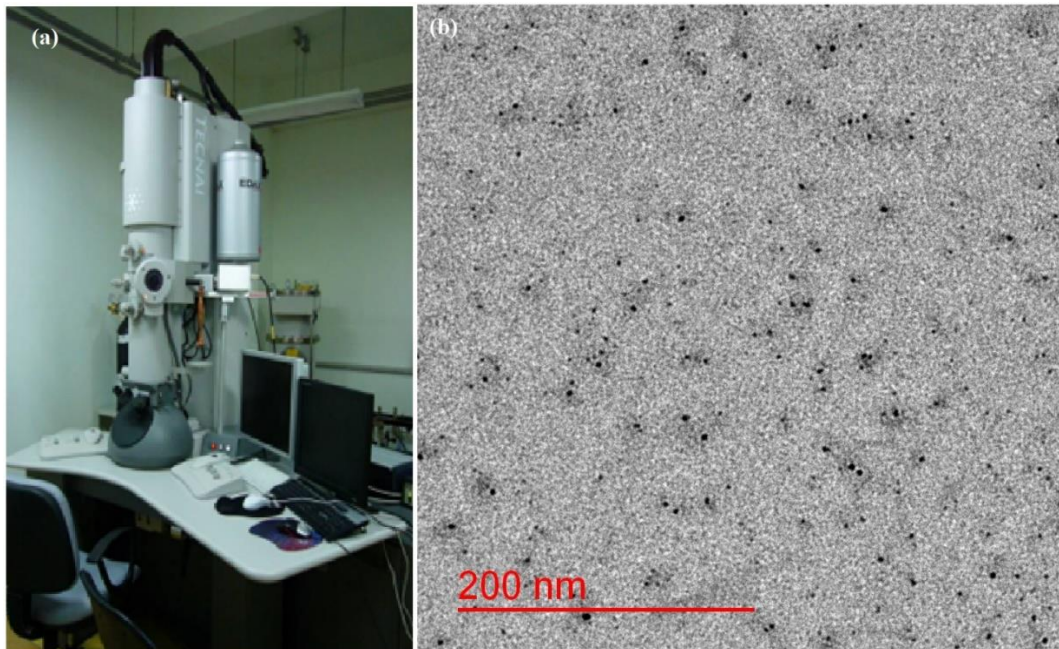Figure 2.10 Schematic diagram of TEM

Figure 2.11 (a) Schematic diagram of HR-TEM, (b) HR-TEM image of N-CDs.

2.3.7 UV- Visible spectroscopy

The Ultra Violet-visible (UV-Vis) absorbance spectra of materials are recorded with the use of a Spectrophotometer, and the optical band gap is estimated with the help of the well-known Tauc equation. The absorbance coefficient and the optical band gap are used in the Tauc relation $(h\nu)^2 = A(h-E_g)$, where 'h' is plank's constant and " is frequency. This relationship is used to determine the optical band gap. In the course of working on this thesis, we made use of a Horiba Jobin Yvon spectrophotometer to record the UV-Vis spectra of a number of different materials[87]. The Figure 2.12 shows the schematic diagram of the UV-Vis spectroscopy and Image of the instrument with Figure 2.12 (c) data plot out from the instrument.
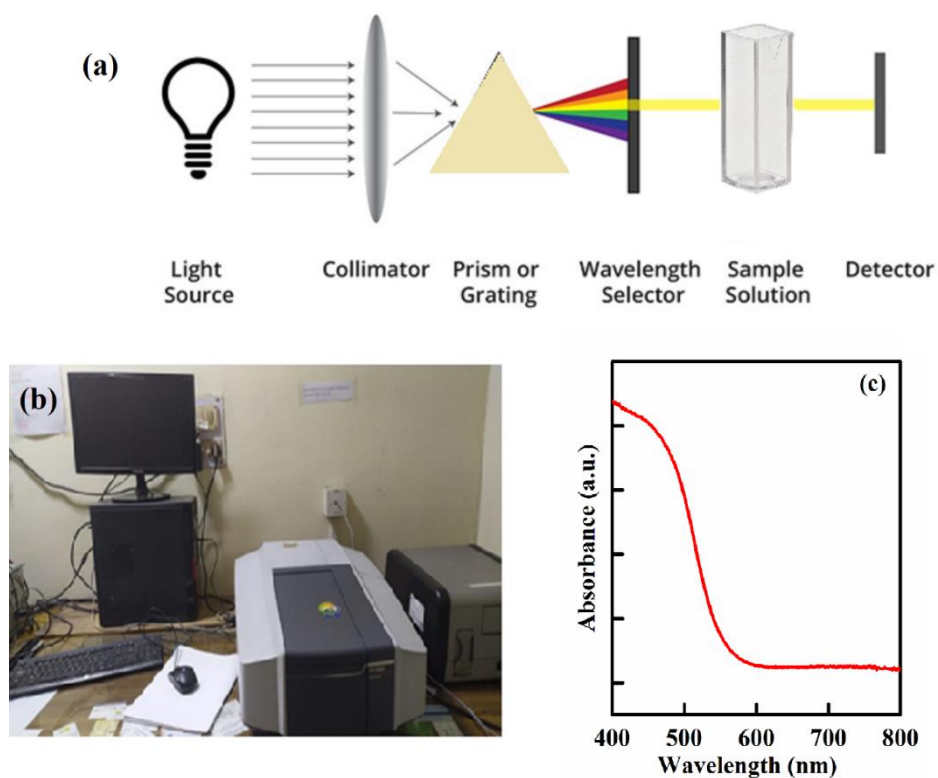

Figure 2.12 (a) Schematic diagram of UV-Visible spectroscopy, (b) PL instrument and (c) data plot of UV spectrum of the sample.

2.3.8 Atomic Force Microscopy

Atomic force microscopy (AFM) technique is widely used advanced characterization method to investigated the surface morphology of the thick or thin films surfaces. An AFM unit consists of a cantilever with a silicon tip, a photo-detector, laser diode, scanner and feedback loop, as shown schematically in Figure 2.13. The tip is attached to the end of cantilever. The AFM tips are made from silicon. When the tip approaches near the surface of sample, the inter-atomic forces between atom at sample surface and atom at AFM tip generates a measurable deflection of the cantilever. AFM measures the vertical deflection of the cantilever with picometer resolution. In this system, the laser beam reflected from the backside of the AFM cantilever is detected on to a position sensitive photodetector to measure the AFM tip deflection. If the cantilever moves just a little bit, the reflected beam will tilt and move around on the photodetector [88]. Images are made by keeping track of how the forces between the tip and the surface of the sample change as the cantilever is moved over the sample. The Figure 2.13 shows Schematic diagram of AFM, Instruments image and 3D micrograph of PVDF surface got from the AFM with the help of NOVO Software.
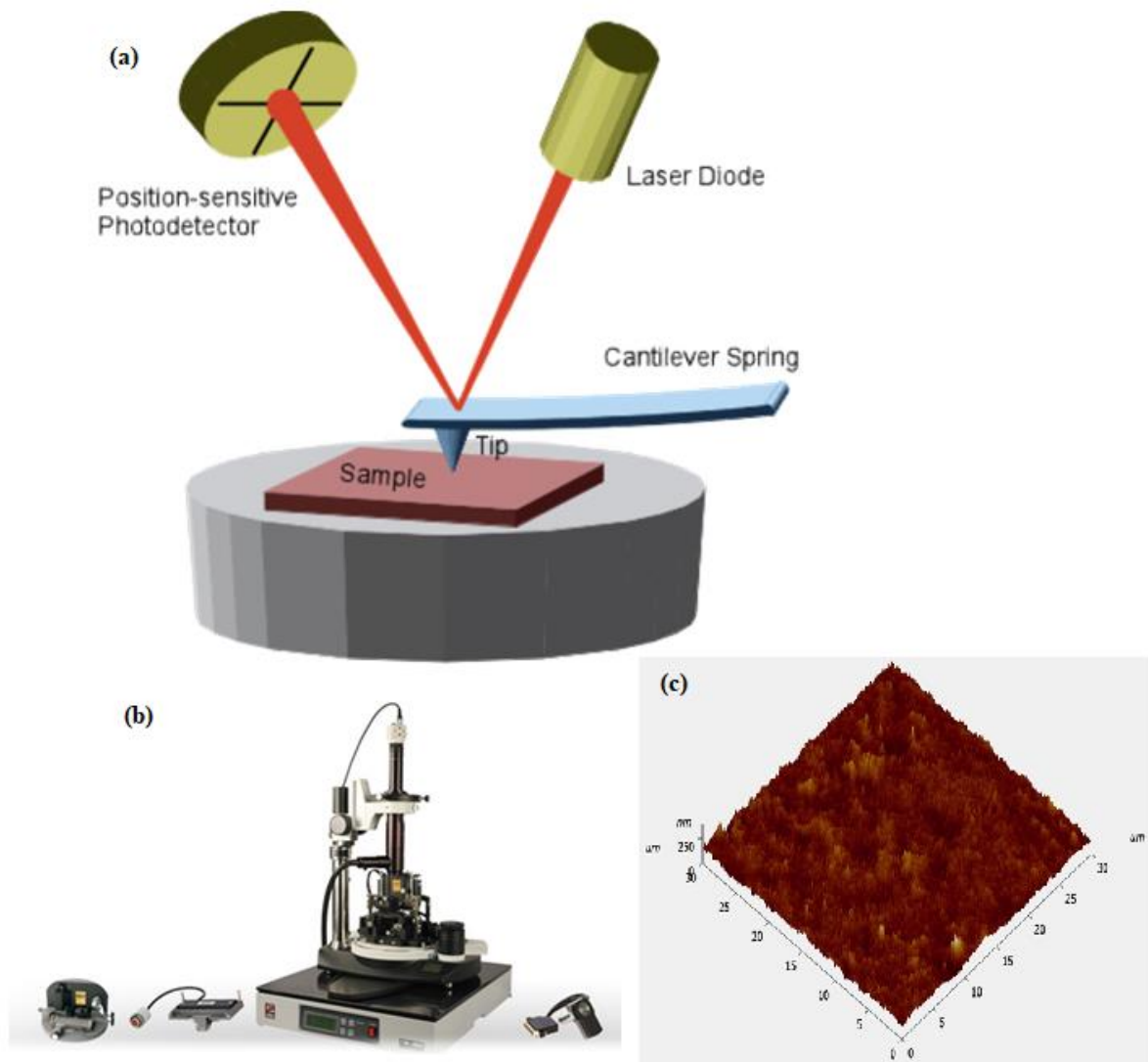
Figure 2.13 (a) Schematic diagram of AFM, (b) Instruments and (c) 3D micrograph of PVDF surface got from the AFM with the help of NOVO Software.

2.3.9   Impedance Spectroscopy

The Figure 2.14 shows the circuit diagram impedance spectroscopy and image of the instrument with the data plot. Dielectric permittivity (ε_r) of a material indicates how easily an electric field may polarize it. dielectric constant (relative permittivity) of Material indicates its capacitive energy storage. Permittivity is real and imaginary. Dielectric loss ($\tan\delta$) is the ratio of imaginary to real part of the permittivity. In this thesis, dielectric constant, dielectric-loss, and resistive behavior were measured at various frequencies and temperatures using a

Keysight-E4990A impedance analyzer. Parallel plate capacitor is made of sample to measure the dielectric capacitance. The sample forms a capacitor sandwiched between upper to bottom Ag- electrodes. The capacitance is measured with varying frequency and temperature and further this capacitance is converted to various parameters including dielectric constant, dielectric loss with the help of AGILANT software installed in the attached desktop. Most of the evaluated samples had dielectric constant and dielectric loss measured from 100 Hz to 1MHz. Parallel plate capacitor capacitance formula $C = \varepsilon_r\varepsilon_0 A/d$, where r is the relative permittivity of the dielectric material, 0 is the permittivity (ε_0) of empty space, A is the electrode area, and d is the dielectric thickness between parallel electrode plates.
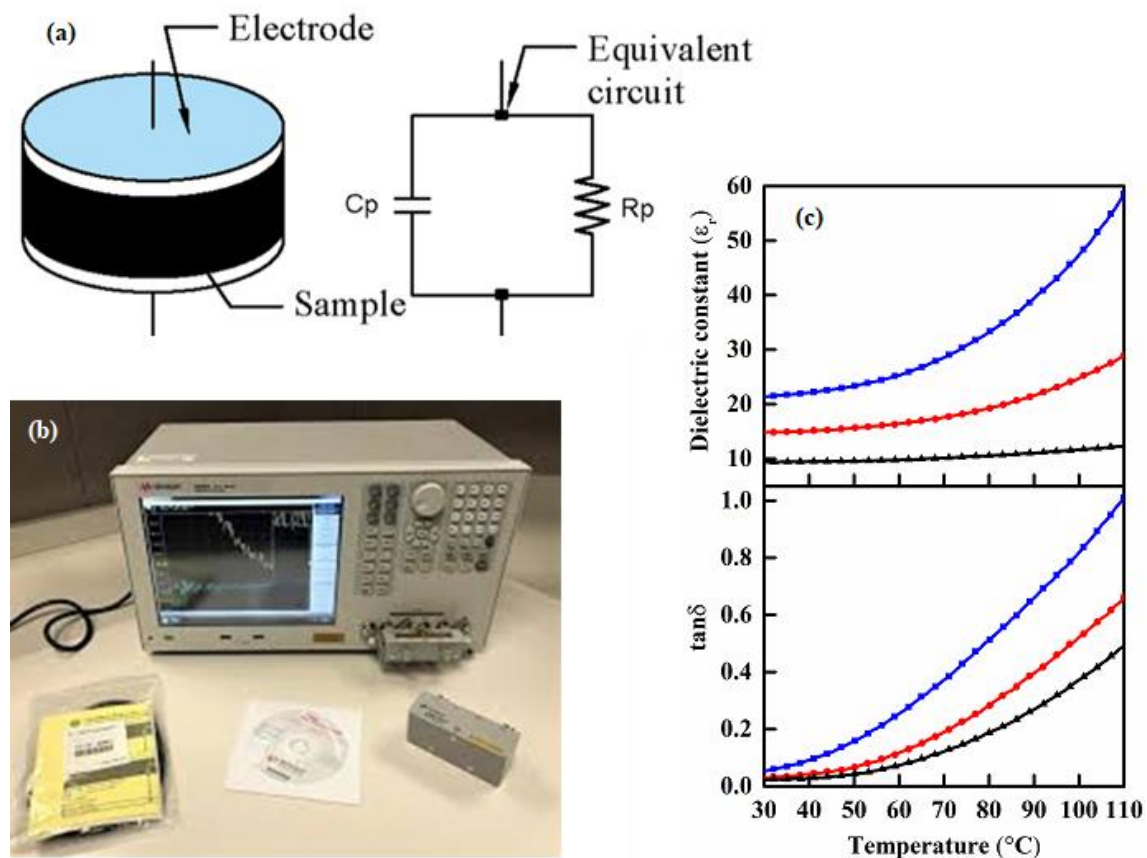

Figure 2.13 (a) Basic circuit diagram of Impedance spectroscopy, (b) Keysight instrument image and (c) Dielectric constant and temperature plot of the sample.

2.3.10 Polarization-Electric field hysteresis loop characterization

Spontaneous polarization is a need for ferroelectric materials. P-E hysteresis loop measures ferroelectric behavior. Figure 2.20 shows the P-E hysteresis loop based on the Sawyer-Tower circuit. Signal generators cycle voltage during P-E loop measurements. In Sawyer-Tower, a ferroelectric capacitor (sample) is coupled to a reference capacitor. The polarization 'P' is calculated as P= Q/A = (C*V/A), where 'Q' is the capacitor charge, which is the same on both capacitors as they are linked in series, 'A' is the sample electrode area, and 'V' is the voltage across the reference capacitor, which is monitored using an oscilloscope. P-E loop provides leftover polarization and coercive field. This experiment studied ferroelectric polarization as a function of external field using Radiant Technologies' Precision Premier-II ferroelectric tester. P-E hysteresis loops were recorded at room temperature and different temperatures. P-E loops are measured using 1Hz to 1kHz sinusoidal ac-voltage.
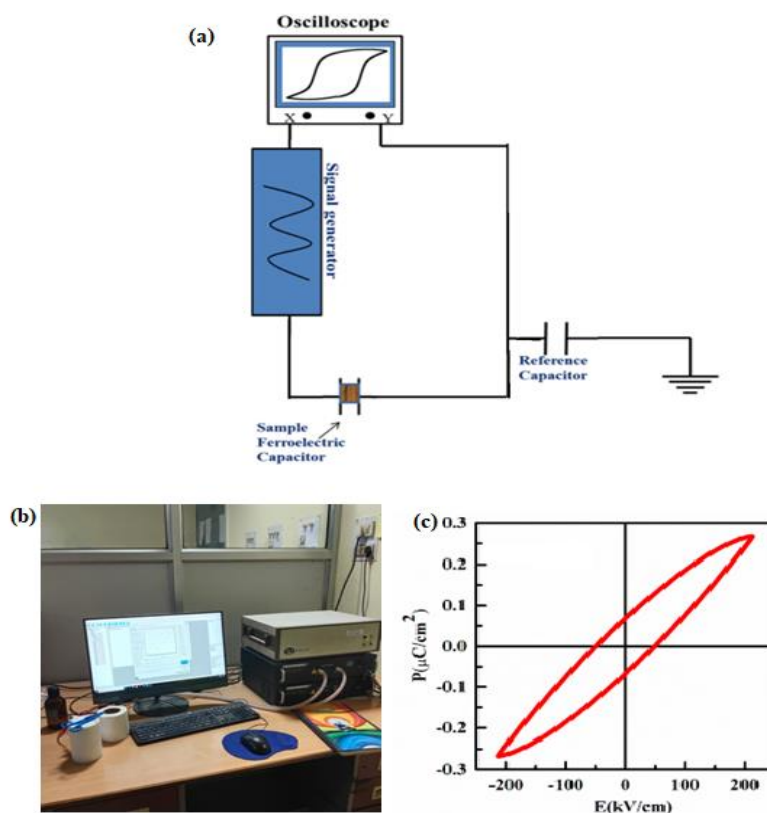

Figure 2.14 (a) Schematic Sawyer-Tower circuit for measurement of ferroelectric polarization, (b) The Radiant PE loop analyzer.

2.3.11 AC Test set up

The breakdown strength of the PVDF and nanocomposite films was measured with the help of the AC High Voltage Test Set-up made by the Neo Tele-Tronix Pvt. Ltd, Kolkata, India (NTPL). HV transformer is major component in this set up with the control and measuring circuits, additionally Reactor (Fixed / Variable), capacitive potential divider and numerous other components could be added as required capacity. The output supply to the sample is from 0 to 500kV continuously varying with the current varying from mA range to 20A for the Intermittent (5min On, 10min Off). HV Transformers that are of an appropriate capacity and are of the cast resin/Oil Cooled Indoor kind. The high-voltage winding has a graded insulation, and one end is linked to the earth potential through a CT. while the other end continues to function as an H.T. floating situation while an ammeter and tripping device are being operated. terminal. Voltage Regulator is used to supply continuously variable and suitable capacity. The transformer will be built to resist frequent intermittent in over & short circuit situation in which such testing transformers are meant to work. Circuitry for controlling the rise and decrease of the test voltage. Interlocking of the limit switch's minimum and maximum positions, which, when engaged, immediately disconnects the increase/decrease circuit mode. In order to prevent having a power factor that is too low and to compensate for the mains supply current due to the DUT primarily being capacitive, a reactor (variable, shunt) is used. When substantial capacitive loading is present, an HV capacitive potential divider is used. The HV Output measurement obtained from the LT side or the Tertiary Winding may not correspond to the predicted voltage. In order to get an accurate reading, a capacitive high-voltage potential divider that is outfitted with a low-voltage arm may be attached directly. Connecting to a metering circuit that displays high voltage requires the use of a UHF connection in conjunction with a co-axial cable. The capacitor will be of the oil-cooled kind, equipped with a corona guard, and will either be stationary or moveable, with wheels located at its base. For greater capacity test sets consisting

of many units, it is possible to mount them on a structure provided that the structure has a lifting arrangement and the appropriate sheet steel cover. It is possible to relocate the structure from one location to another without having to pack it up or re-establish connections between the individual pieces. Image of the instrument is shown in the Figure 2.16 (a) with the Punctured nanocomposite sample after breakdown
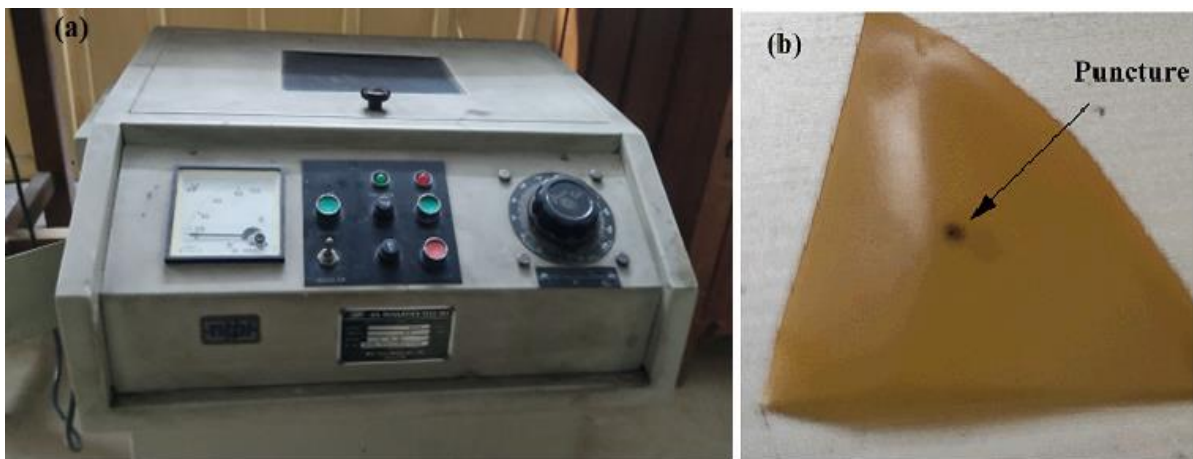

Figure 2.15 (a) Image of Instrument AC Test set up, (b) Punctured nanocomposite sample after breakdown.

2.7. Conclusions

In this chapter we have discussed the materials and method in detail. The general synthesis process of the nanoparticles and nanocomposite films. The hydroxylation of the nanoparticles also discussed. The characterization techniques of the samples prepared have been discussed. The details of instruments mechanism and working principle is discussed. The plotting of the data is shown with the image of instruments. In the upcoming chapter, the investigation of the data from the sample of ferroelectric films.